

Effect of interfacial species mixing on phonon transport in semiconductor superlattices

E. S. Landry and A. J. H. McGaughey*

Department of Mechanical Engineering, Carnegie Mellon University, Pittsburgh, Pennsylvania 15213, USA

(Received 12 December 2008; published 19 February 2009)

Molecular dynamics simulations are used to examine the effect of interfacial species mixing on the thermal conductivity of Stillinger-Weber Si/Si_{0.7}Ge_{0.3} and Si/Ge superlattices at a temperature of 500 K. The thermal conductivity of Si/Si_{0.7}Ge_{0.3} superlattices is predicted to not depend on the interfacial species mixing and to increase with increasing period length. This period length dependence is indicative of incoherent phonon transport and related to decreasing interface density. The thermal conductivity of Si/Ge superlattices is predicted to depend strongly on the interface quality. For Si/Ge superlattices with perfect interfaces, the predicted thermal conductivity decreases with increasing period length before reaching a constant value, a trend indicative of coherent phonon transport. When interfacial species mixing is added to the model, however, the thermal conductivity is predicted to increase with increasing period length, indicating incoherent phonon transport. These results suggest that the assumption of coherent phonon transport made in lattice dynamics–based models may not be justified.

DOI: [10.1103/PhysRevB.79.075316](https://doi.org/10.1103/PhysRevB.79.075316)

PACS number(s): 68.65.Cd, 65.40.–b, 63.22.Np

I. INTRODUCTION

A superlattice is a periodic nanostructure built from epitaxial material layers with thicknesses as small as a few nanometers.¹ Semiconductor superlattices are the focus of much research due to their potential to increase the efficiency of thermoelectric energy conversion devices.^{2–4} The thermodynamic efficiency of thermoelectric energy conversion is related to the thermoelectric figure of merit ZT , which itself is inversely proportional to thermal conductivity.^{2,4} Si/Si_{1–x}Ge_x superlattices are especially promising for increasing ZT because their cross-plane thermal conductivities can be less than values for alloys of the same composition^{5–7} (which themselves are good thermoelectric materials^{2,3,8}).

The effect of unit-cell design on the cross-plane thermal conductivity of Si/Si_{1–x}Ge_x superlattices has been systematically examined in only a few^{5,6,9} of the experimental studies.^{5–7,9–12} In each of these studies, the thermal-conductivity dependence on period length was examined for superlattices that contained two layers in the unit cell. Based on our recent study of model Lennard-Jones superlattices,¹³ we believe that the lowest thermal conductivities will be realized for superlattices with unit cells that contain more than two layers. In order to guide the design of such superlattices, however, accurate and reliable thermal transport modeling tools are required. Of particular importance is the ability of these models to account for deviations from perfect interface quality as will be found in realistic superlattices.^{14–16}

The most common modeling approaches are rooted in the Boltzmann transport equation (BTE) (Refs. 17 and 18) and lattice dynamics calculations,^{19–27} both of which require many assumptions. In the BTE approach, phonons are treated as particles and their wavelike nature is neglected. This treatment requires that the phonon populations in neighboring layers be uncorrelated (i.e., incoherent phonon transport), valid when the phonon mean free path is less than the superlattice layer thicknesses. In addition, the nature of the phonon scattering within the layers (e.g., phonon relaxation times) and at interfaces must be specified *a priori*. The BTE

approach predicts the primary resistance to thermal transport to be phonon scattering at interfaces,^{17,18} leading to a trend of increasing thermal conductivity with increasing period length due to decreasing interface density.

Lattice dynamics calculations require that the phonon populations in neighboring layers be coherently correlated and that the samples be perfectly periodic. The phonon populations will be coherently correlated when the phonon mean free path is greater than the superlattice period length. This assumption can be relaxed in a phenomenological manner to include incoherent effects by adding an imaginary component to the phonon wave vector.^{25,26} The requirement that the samples be perfectly periodic eliminates the modeling of alloys or deviations in superlattice interface quality,²⁸ both of which are common in applications. Traditional lattice dynamics calculations are performed under the harmonic approximation.^{20–27} Under this approximation, the phonon modes are decoupled and, thus, the nature of the phonon scattering must be specified. Typically, the phonon relaxation times are assumed to be phonon mode and superlattice independent.^{20–24,27} Broido and Reinecke¹⁹ used an anharmonic lattice dynamics–based approach to calculate the phonon mode–specific relaxation times for Si/Ge superlattices. They found that the assumption of a phonon mode– and superlattice-independent relaxation time is poor and predicted the thermal conductivity of short-period Si/Ge superlattices to decrease with increasing period length.¹⁹

The predictive power of the BTE- and lattice dynamics–based approaches is limited due to the many assumptions underlying them. An alternative approach is molecular dynamics (MD) simulation, which can explicitly model interface quality and requires no assumptions about the nature of phonon transport. In a MD simulation, the time evolution of the positions and momenta of a set of atoms is predicted using the Newtonian equations of motion. Such simulations have been applied to model superlattice systems,^{13,29–34} as reviewed in our recent work.¹³ To our knowledge, however, there has been only one limited study using MD to predict the thermal conductivity of Si/Ge superlattices.³⁵

In this work, MD simulations are used to predict the effect of interfacial species mixing on the cross-plane thermal conductivity of two types of Si/Si_{1-x}Ge_x superlattices. For comparison, we also predict the thermal conductivities of Si_{1-x}Ge_x alloys. Using these predictions, we assess the role of phonon coherence on the thermal transport in superlattices.

II. MOLECULAR DYNAMICS SIMULATIONS

A. Interatomic potential and simulation methodology

The primary input to a MD simulation is an interatomic potential for modeling the atomic interactions. We use the Stillinger-Weber (SW) interatomic potential, which has been parameterized for both Si and Ge.^{36,37} For the Si-Ge interactions, we use the mixing rules described by Laradji *et al.*³⁸ While the SW potential has been widely used for modeling Si- and Ge-based materials,^{35–37,39–43} it has several deficiencies that influence its quantitative accuracy for modeling thermal transport. For example, the slopes of the high-symmetry transverse-acoustic phonon dispersion branches in SW Si and Ge are too high (leading to overpredictions of the phonon group velocities),^{37,44} and the experimental Grüneisen parameters are not well reproduced.⁴⁴ In light of these deficiencies, we will compare our MD predictions to experimental measurements on a qualitative basis. Any quantitative agreement would be fortuitous.

The velocity Verlet algorithm is used to integrate the Newtonian equations of motion with a time step of 0.55 fs. Because MD simulation is only strictly valid in the classical limit, the thermal conductivity predictions are made at a temperature T of 500 K. Quantum effects are expected to be negligible at this temperature because it is close to or greater than the Debye temperatures of 708 and 429 K for SW Si and Ge.⁴⁵

B. Sample preparation

We will predict the thermal conductivities of Si_{1-x}Ge_x alloys and two types of Si/Si_{1-x}Ge_x superlattice. The two types of superlattice have been experimentally characterized^{5,9} and are: (i) Si/Si_{0.7}Ge_{0.3} with the Si layer being twice as thick as the alloy layer, and (ii) Si/Ge with equal Si and Ge layer thicknesses. We refer to a particular superlattice in the format $m \times n$, where m and n are the number of monolayers of the first and second materials. The 32×16 Si/Si_{0.7}Ge_{0.3} and 24×24 Si/Ge superlattices are shown in Fig. 1 along with their period lengths L . For both types of superlattice, we consider a range of period lengths similar to those that have been experimentally characterized.^{5,9} Note that the interfaces are parallel to the (001) crystallographic plane (i.e., the xy plane). In all of the samples, the mass and species of each atom are randomly assigned according to the natural isotope abundance⁴⁶ for Si or Ge and the desired fraction of Ge (x).

The thermal conductivity predictions are made using relaxed, zero-pressure samples. The zero-pressure simulation cell dimensions are determined from separate MD simulations run at constant temperature and pressure using a Nose-Hoover thermostat⁴⁷ and a Berendsen barostat⁴⁸ with inde-

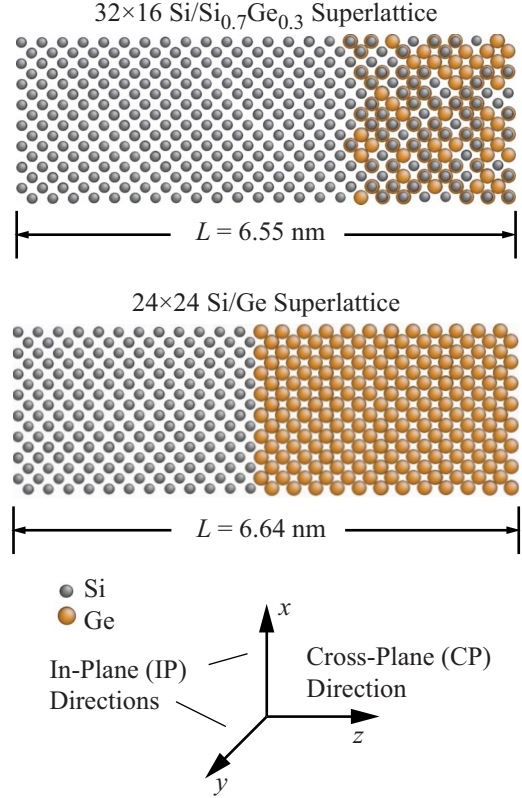


FIG. 1. (Color online) One period of the 32×16 Si/Si_{0.7}Ge_{0.3} and 24×24 Si/Ge superlattices with perfect interfaces.

pendent control of stress in each direction. For the Si_{1-x}Ge_x alloy, we find that the zero-pressure lattice constant a at a temperature of 500 K is approximated to within 0.01% over the entire x range ($0 \leq x \leq 1$) by

$$a(x) = 5.441 + 0.226x + 0.003x^2 \text{ (\AA)}. \quad (1)$$

For the Si/Si_{1-x}Ge_x superlattices, the lattice constant that leads to zero stress in the in-plane directions (the x and y directions) lies between the bulk lattice constants for Si and the Si_{1-x}Ge_x alloy. This configuration results in symmetrically strained superlattices in which the tensile stress in the Si layers balances the compressive stress in the Si_{1-x}Ge_x layers. Due to the in-plane strain within each layer, the lattice constants that lead to zero cross-plane (the z -direction) stress are also different from the bulk Si and Si_{1-x}Ge_x alloy lattice constants. The Si layer is negatively strained and the Si_{1-x}Ge_x layer is positively strained in the cross-plane direction. We find that the zero-stress lattice constants obtained from our MD simulations are in good agreement with those predicted from elasticity theory and the SW elastic constants.¹⁴

C. Interfacial species mixing

Realistic superlattices contain defects due to: (i) interfacial species mixing, (ii) epitaxial layer roughening, and (iii) misfit dislocations.^{14–16} In Si/Si_{1-x}Ge_x superlattices, the defects exist to release the strain energy associated with the lattice mismatch between Si and Si_{1-x}Ge_x. While each defect

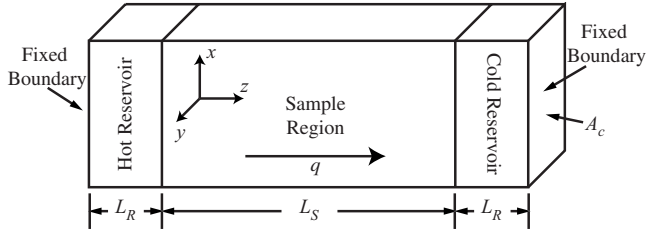


FIG. 2. Schematic of the simulation cell used in the direct method.

type will influence the superlattice thermal conductivity, epitaxial layer roughening and misfit dislocations cannot be directly modeled with MD because they require prohibitively large simulation cells.⁴⁹ We can, however, examine the effect of interfacial species mixing to begin to elucidate the effects that deviations from perfect sample quality have on the nature of the phonon transport in superlattices.

We include interfacial species mixing in the superlattice samples by randomly assigning the species of each atom in the interface region according to the distribution

$$x(z) = x_L + \frac{1}{2}(x_R - x_L) \left[1 + \tanh\left(\frac{4z}{D}\right) \right]. \quad (2)$$

Here, D is the interface thickness (i.e., the thickness of the species mixing region), z is measured relative to the closest interface, and x_L and x_R are the desired unmixed Ge concentrations on the left ($z < 0$) and right ($z > 0$) sides of the interface. The Ge concentration curve produced by Eq. (2) is similar in shape to experimental observations for Si/Si_{1-x}Ge_x superlattices.⁵⁰ We will compare the thermal conductivities of superlattices with atomically perfect interfaces to those with $D=2$ monolayers, which results in species mixing primarily in the first monolayer on either side of each interface. For example, in the Si/Ge superlattices, the average compositions of the Si and Ge monolayers on either side of the interface become Si_{0.88}Ge_{0.12} and Si_{0.12}Ge_{0.88}.

III. THERMAL CONDUCTIVITY PREDICTION

A. Direct method

The thermal conductivities are predicted using the direct method.^{13,40,51} In this method, a known heat flux q is applied across the sample and the resulting temperature gradient $\partial T/\partial z$ is measured. The thermal conductivity k is then determined using the Fourier law,

$$k = \frac{-q}{\partial T/\partial z}. \quad (3)$$

A schematic of the direct method simulation cell is shown in Fig. 2. The system consists of a sample bordered by hot and cold reservoirs and fixed boundaries in the z direction. The reservoirs have the same composition and periodicity (where applicable) as the sample. The fixed boundary regions each contain four monolayers of fixed atoms in order to prevent reservoir atoms from sublimating. Periodic boundary conditions are imposed in the x and y directions. Our direct

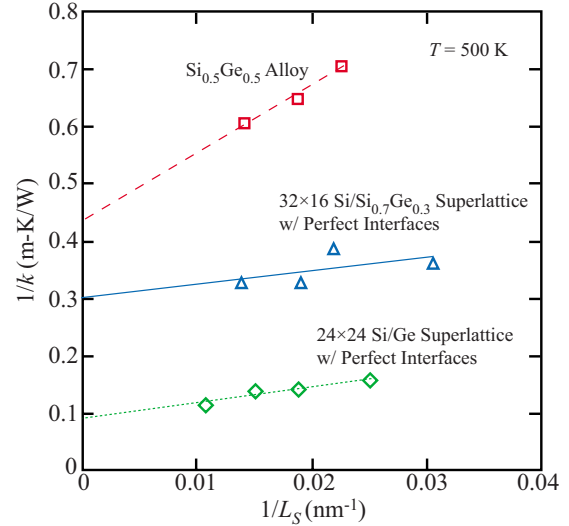


FIG. 3. (Color online) Inverse of the predicted thermal conductivity versus inverse of the total sample length. Finite-size effects are removed by extrapolating to an infinite system size ($1/L_S \rightarrow 0$).

method simulation cells contain between 16 640 and 43 264 atoms.

B. Finite simulation cell-size effect

One challenge associated with the direct method is to obtain thermal conductivity predictions that are independent of the simulation cell size. For example, when the sample length L_S is on the order of or less than the bulk phonon mean free path, the amount of phonon scattering at the boundaries between the reservoirs and the sample is comparable to that occurring within the sample itself. Furthermore, phonons can potentially travel from the hot reservoir to the cold reservoir without scattering (i.e., ballistic transport). Both of these effects lead to phonon dynamics not representative of a bulk sample and a dependence between the thermal conductivity and the sample length.

The method used here to remove the thermal conductivity dependence on sample length was described by Schelling *et al.*⁴⁰ and in our previous work.¹³ It is based on the prediction obtained from the Matthiessen rule and the kinetic theory expression for thermal conductivity that the inverse of the thermal conductivity decreases linearly with the inverse of the sample length.⁴⁰ The thermal conductivity corresponding to a sample of infinite length can therefore be determined by extrapolating to the $1/L_S \rightarrow 0$ limit. This method is illustrated in Fig. 3 for the Si_{0.5}Ge_{0.5} alloy and the 24 × 24 Si/Ge and 32 × 16 Si/Si_{0.7}Ge_{0.3} superlattices with perfect interfaces. In all cases, the trend of $1/k$ versus $1/L_S$ is linear, verifying the use of the extrapolation method to remove the finite-sample-size effect.

We find that the thermal conductivity is independent of the cross-sectional area A_c (see Fig. 2) when this area is greater than or equal to four unit cells by four unit cells, in agreement with the findings of Schelling *et al.*⁴⁰ for bulk Si. This independence implies that the resolution of the Brillouin zone in the x and y directions is fine enough so as not to affect thermal transport in the z direction.

TABLE I. Applied heat flux (q), time allowed to reach steady-state conditions (τ_{ss}), and time used for the thermal conductivity prediction (τ_{av}).

Sample	q (GW/m ²)	τ_{ss} (ns)	τ_{av} (ns)
Si _{1-x} Ge _x alloys	3.10	3.3	1.1
Si/Si _{0.7} Ge _{0.3} superlattices	6.19	3.3	1.1
Si/Ge superlattices	6.19	2.8	2.8

The thermal conductivity also depends on the reservoir length L_R . The reservoir length limits the phonon wavelengths that can propagate from the reservoir to the sample. Small reservoirs may therefore produce unrealistic phonon distributions. Furthermore, most methods of applying the heat flux (including the method used here; see Sec. III C) involve scaling the velocities of the reservoir atoms to add or remove a desired amount of kinetic energy. Having a large number of atoms in the reservoir is thus preferred because it reduces the required energy change per atom, minimizing non-Newtonian dynamics. We have examined the reservoir size effect for bulk Si at a temperature of 500 K and found the thermal conductivity to depend on L_R even when it is as large as 128 monolayers.⁵² The extrapolated thermal conductivity, however, was found to be independent of the reservoir length when it was greater than or equal to 128 monolayers. For all the samples considered here, which should have reduced size effects compared to Si due to their lower thermal conductivities (and, thus, smaller phonon mean free paths), the reservoir length is at least 128 monolayers.⁵³

C. Data collection and analysis

The sample and reservoirs are initially set to a uniform temperature of 500 K by scaling the atomic velocities for 0.55 ns (1×10^6 time steps). The heat flux is then applied across the sample. The heat flux is generated by adding a constant amount of kinetic energy to the hot reservoir and removing the same amount of kinetic energy from the cold reservoir at every time step using the method described by Ikeshoji and Hafskjold.⁵⁴ With this method, the positions and momenta of the atoms within the sample are allowed to evolve naturally.

From the point when the heat flux is first applied, a period of time τ_{ss} is allowed for the sample to reach steady-state conditions. After this period, data are collected over an additional time period of τ_{av} for the thermal conductivity prediction. The τ_{ss} and τ_{av} values are provided for each sample type in Table I. We estimate that the τ_{av} values result in a thermal conductivity prediction uncertainty of $\pm 20\%$. This estimate is based on our ability to specify the temperature gradient for each sample size and the scatter in the extrapolation line used to remove the finite-sample-length effect (see Fig. 3).

The value of the heat flux should be chosen so that the temperature drop across the sample is large enough to accurately specify the temperature gradient. It should not be so large, however, that nonlinear temperature profiles are intro-

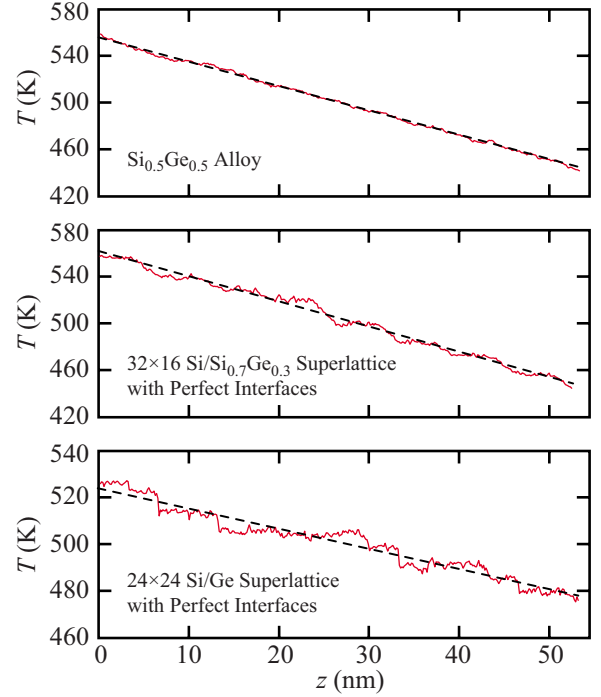


FIG. 4. (Color online) Temperature profile (solid red line) and linear fit (dashed black line) in the sample region for the Si_{0.5}Ge_{0.5} alloy, and the 24 × 24 Si/Ge and 32 × 16 Si/Si_{0.7}Ge_{0.3} superlattices with perfect interfaces. The sample length for all of these cases is between 52.4 and 53.3 nm (384 monolayers). Note the differences in the temperature scale for each plot.

duced due to the temperature dependence of the thermal conductivity. The heat flux values that meet these requirements are provided in Table I. The temperature profiles within samples of a Si_{0.5}Ge_{0.5} alloy and 24 × 24 Si/Ge and 32 × 16 Si/Si_{0.7}Ge_{0.3} superlattices with perfect interfaces (each with a length of 384 monolayers) are provided in Fig. 4 as examples. The temperature profiles are linear in each case, despite the large temperature drops. This result indicates that the thermal conductivities of Si_{1-x}Ge_x alloys and Si/Si_{1-x}Ge_x superlattices are weakly dependent on temperature in this temperature range.

When making the thermal conductivity prediction, the temperature of each atomic layer is found by averaging over τ_{av} , and the temperature gradient is specified by applying a least-squares linear regression analysis to the resulting temperature profile. The linear fits for the Si_{0.5}Ge_{0.5} alloy and the 24 × 24 Si/Ge and 32 × 16 Si/Si_{0.7}Ge_{0.3} superlattices with perfect interfaces are provided in Fig. 4. We have observed nonlinear temperature profiles for simulations of bulk Si and Ge near the reservoir/sample interfaces due to phonon scattering at these interfaces,⁵² in agreement with the observation of Schelling *et al.*⁴⁰ Because this nonlinear effect is not present for the alloy and superlattice samples, we include the entire sample when specifying the temperature gradient. We found that the nonlinear effect is more pronounced in the superlattices when the reservoirs contain one of the bulk species rather than maintain the superlattice periodicity. We therefore use reservoirs that maintain the superlattice periodicity, allowing more data to be used for the temperature gradient specification.

TABLE II. Molecular dynamics-predicted thermal conductivities for $\text{Si}_{1-x}\text{Ge}_x$ alloys.

Germanium concentration x	Predicted k (W/m K)
0.125	2.6 ± 0.5
0.250	2.4 ± 0.5
0.375	2.0 ± 0.4
0.500	2.3 ± 0.5
0.625	3.4 ± 0.7
0.750	4.2 ± 0.8
0.875	6.1 ± 1.2

IV. RESULTS

A. $\text{Si}_{1-x}\text{Ge}_x$ alloy

One way in which the ZT of a $\text{Si}/\text{Si}_{1-x}\text{Ge}_x$ superlattice can be increased above the values associated with the $\text{Si}_{1-x}\text{Ge}_x$ alloy is for its thermal conductivity to be reduced below that of an alloy with the same Ge concentration. We therefore predict the thermal conductivities of $\text{Si}_{1-x}\text{Ge}_x$ alloys to allow for comparison to our predicted superlattice thermal conductivities, which are presented in Secs. IV B and IV C.

The predicted thermal conductivities for the $\text{Si}_{1-x}\text{Ge}_x$ alloys at a temperature of 500 K are provided in Table II. The alloy thermal conductivity decreases with increasing Ge concentration until $x=0.375$, beyond which it increases with increasing Ge concentration. A minimum alloy thermal conductivity for a Ge concentration less than 0.5 is in agreement with experimental measurements for $\text{Si}_{1-x}\text{Ge}_x$ alloys at a temperature of 300 K (limited experimental data are available at a temperature of 500 K). Our predicted alloy thermal conductivities are greater than the values recently predicted by Skye and Schelling⁵⁵ using MD simulation and the SW potential. We attribute this difference to finite-cell-size effects present in their predictions (i.e., they did not apply the extrapolation procedure discussed in Sec. III B).

B. $\text{Si}/\text{Si}_{0.7}\text{Ge}_{0.3}$ superlattices

The MD-predicted thermal conductivities for $\text{Si}/\text{Si}_{0.7}\text{Ge}_{0.3}$ superlattices with perfect interfaces and with interfacial species mixing are plotted against the superlattice period length in Fig. 5. The thermal conductivity of an alloy with the same Ge concentration (i.e., the $\text{Si}_{0.9}\text{Ge}_{0.1}$ alloy, extrapolated from the data in Table II) is provided for comparison. In all cases, the superlattice thermal conductivities are greater than the corresponding alloy value. The superlattice thermal conductivities increase with increasing period length, a trend indicative of incoherent phonon transport and related to decreasing interface density.^{17,18} This result is expected because these superlattices lack perfect periodicity due to the disordered alloy layers, limiting the formation of coherent Bloch phonons to those with very long wavelengths (i.e., the elastic limit). In addition, the thermal conductivity of each $\text{Si}/\text{Si}_{0.7}\text{Ge}_{0.3}$ superlattice with perfect interfaces is within the

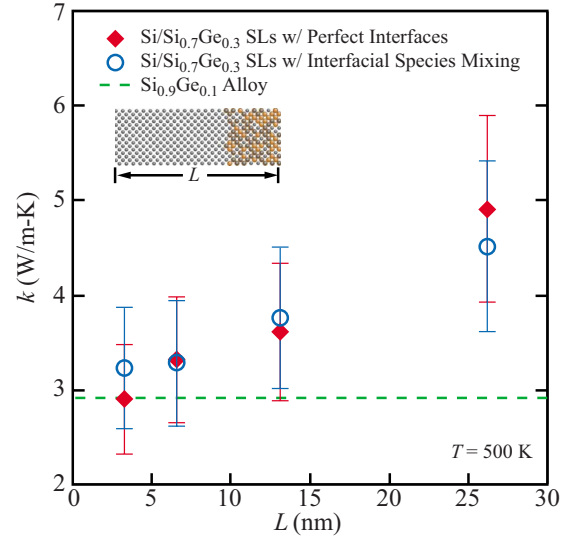


FIG. 5. (Color online) Molecular dynamics predicted thermal conductivities for $\text{Si}/\text{Si}_{0.7}\text{Ge}_{0.3}$ superlattices with perfect interfaces and with interfacial species mixing. The thermal conductivity of the alloy with identical average composition (the $\text{Si}_{0.9}\text{Ge}_{0.1}$ alloy) is provided for comparison.

prediction uncertainty of the corresponding structure with interfacial species mixing. We attribute this result to the fact that the $\text{Si}/\text{Si}_{0.7}\text{Ge}_{0.3}$ interfaces are disordered even before the introduction of interfacial species mixing.

Our predicted trends of (i) increasing thermal conductivity with increasing period length and (ii) superlattice thermal conductivities greater than the corresponding alloy value are in qualitative agreement with the experimental measurements of Huxtable⁹ made at a temperature of 320 K (the highest temperature available) for similar $\text{Si}/\text{Si}_{0.7}\text{Ge}_{0.3}$ superlattices. While the MD predictions and experimental measurements correspond to different temperatures, we believe that the data can still be compared because the superlattice thermal conductivity is experimentally observed to depend weakly on temperature above 200 K.⁹

C. Si/Ge superlattices

The predicted thermal conductivities for Si/Ge superlattices with perfect interfaces and with interfacial species mixing are shown in Fig. 6 as a function of superlattice period length. The thermal conductivity of the alloy with the same Ge concentration (the $\text{Si}_{0.5}\text{Ge}_{0.5}$ alloy) is provided for comparison. For Si/Ge superlattices with perfect interfaces, we predict the thermal conductivity to decrease with increasing period length and then reach a constant value of ~ 12 W/m K for period lengths greater than or equal to 6.64 nm. This trend is in qualitative agreement with that calculated by Broido and Reinecke¹⁹ for Si/Ge superlattices with perfect interfaces using an anharmonic lattice dynamics-based model under the assumption of coherent phonon transport.

The thermal conductivity dependence on period length is different when interfacial species mixing is introduced. The thermal conductivities in this case increase with increasing

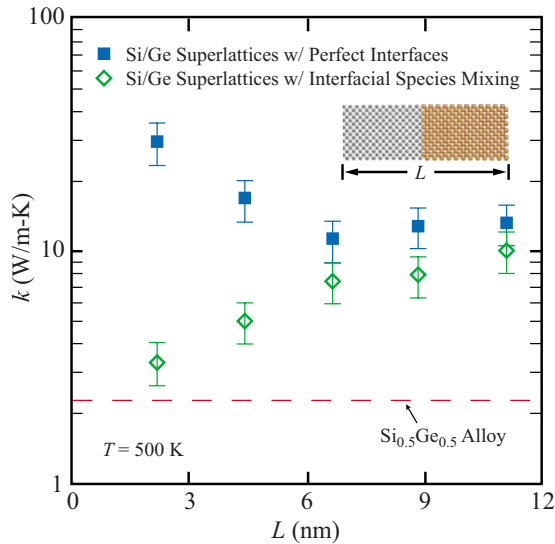


FIG. 6. (Color online) Molecular dynamics predicted thermal conductivities for Si/Ge superlattices with perfect interfaces and with interfacial species mixing. The thermal conductivity of the $\text{Si}_{0.5}\text{Ge}_{0.5}$ alloy is provided for comparison.

period length, indicating incoherent phonon transport.^{17,18} In addition, the magnitude of the thermal conductivity decreases by as much as an order of magnitude compared to the samples with perfect interfaces. These findings are consistent with the MD predictions of Daly *et al.*³² for a simplified model of GaAs/AlAs superlattices.

Experimental measurements of the Si/Ge superlattice thermal conductivity were made by Borca-Tasciuc *et al.*⁵ up to a temperature of 300 K. As with the Si/Si_{0.7}Ge_{0.3} superlattices, the thermal conductivity of Si/Ge superlattices is observed to be independent of temperature above 200 K.⁵ We can therefore compare our MD-predicted trends to the experimental trends at 300 K by assuming that the thermal conductivity remains temperature independent up to a temperature of 500 K.

The experimental thermal conductivity of Si/Ge superlattices is observed to decrease with increasing period length,⁵ a trend similar to that predicted for superlattices in which the phonon transport is coherent.¹⁹ Our MD results indicate, however, that even a small deviation from perfect sample quality, which we have examined here through the introduction of interfacial species mixing, is sufficient to remove the phonon coherence. It is thus unlikely that coherent phonon effects are the mechanism leading to the experimentally observed thermal conductivity dependence on period length. Because the energy associated with the lattice-mismatch strain increases with increasing period length, strain-induced defects (epitaxial layer roughening and misfit dislocations) will increase with increasing period length.^{12,16} Based on our findings, we suggest that phonon scattering at an increasing number of these imperfections leads to the experimental trend of decreasing thermal conductivity with increasing period length.

An additional qualitative difference exists between the MD-predicted and experimentally measured thermal conductivities. While we predict the thermal conductivity of Si/Ge

superlattices to be greater than that of the $\text{Si}_{0.5}\text{Ge}_{0.5}$ alloy, the opposite trend is observed experimentally.⁵ As noted by Kim *et al.*,^{56,57} superlattice thermal conductivities below the alloy value can be a result of a high density of defects.^{9,11,12,56,57} This statement is consistent with our current results and the results of our previous study¹³ of model Lennard-Jones superlattices. For both of these material systems, we predict the thermal conductivities of defect-free superlattices to always be greater than the corresponding alloy value.

V. SUMMARY AND CONCLUSIONS

Molecular dynamics simulations have been used to examine the effect of interfacial species mixing on the thermal conductivity of SW Si/Si_{0.7}Ge_{0.3} and SW Si/Ge superlattices at a temperature of 500 K. In addition, the thermal conductivities of Si_{1-x}Ge_x alloys were predicted for comparison to the superlattice values.

We predict the thermal conductivity of Si/Si_{0.7}Ge_{0.3} superlattices to increase with increasing period length and to be above the value of an alloy with the same Ge composition (see Fig. 5). These findings are in qualitative agreement with experimental data.⁹ The predicted thermal conductivity dependence on period length is indicative of incoherent phonon transport, expected because the disordered alloy layer removes the perfect sample periodicity, thereby preventing the formation of coherent Bloch phonons. The predicted thermal conductivity of each Si/Si_{0.7}Ge_{0.3} superlattice with perfect interfaces is within the prediction uncertainty of the corresponding structure containing interfacial species mixing. This result is due to the internal Si/Si_{0.7}Ge_{0.3} interfaces containing disorder even before the introduction of interfacial species mixing.

The thermal conductivity of Si/Ge superlattices is predicted to depend strongly on the interface quality. For Si/Ge superlattices with perfect interfaces, the predicted thermal conductivity decreases with increasing period length before reaching a constant value (see Fig. 6), a trend similar to that predicted by a lattice dynamics-based model under the assumption of coherent phonon transport.¹⁹ When interfacial species mixing is added to the model, however, we predict the thermal conductivity to increase with increasing period length, a trend indicative of incoherent phonon transport. Because the phonon coherence is removed by deviations from perfect interface quality, we suggest that the experimental observation⁵ of decreasing Si/Ge superlattice thermal conductivity with increasing period length is not due to coherent phonon effects. In all cases, we predict the thermal conductivity of Si/Ge superlattices to be greater than that of the $\text{Si}_{0.5}\text{Ge}_{0.5}$ alloy, a relationship opposite to that observed experimentally. We suggest that this discrepancy, as well as the experimentally observed thermal conductivity dependence on period length, is due to additional phonon scattering at strain-induced defects absent from the MD model.

Due to the predicted sensitivity of the Si/Ge superlattice thermal conductivity on interfacial species mixing, the assumption of coherent phonon transport made in lattice dynamics-based models may not be justified. Instead, BTE-based models, which assume incoherent phonon transport,

may be more appropriate for modeling thermal transport in superlattices. The *a priori* specification of the nature of the phonon scattering within the superlattice layers and at the internal interfaces required by the BTE-based models, however, is still a limitation for their use in guiding the design of superlattices for low thermal conductivity. We believe that, given an accurate interatomic potential, MD simulations can provide the required input (e.g., phonon relaxation times and

phonon-energy transmission coefficients) for the BTE-based models.^{58–61}

ACKNOWLEDGMENTS

This work was supported by the Berkman Faculty Development Fund at Carnegie Mellon University.

*mcgaughey@cmu.edu

- ¹D. G. Cahill, W. K. Ford, K. E. Goodson, G. D. Mahan, A. Mujumdar, H. J. Maris, R. Merlin, and S. R. Phillpot, *J. Appl. Phys.* **93**, 793 (2003).
- ²G. Chen, M. S. Dresselhaus, G. Dresselhaus, J.-P. Fleurial, and T. Caillat, *Int. Mater. Rev.* **48**, 45 (2003).
- ³H. Bottner, G. Chen, and R. Venkatasubramanian, *MRS Bull.* **31**, 211 (2006).
- ⁴M. S. Dresselhaus, G. Chen, M. Y. Tang, R. Yang, H. Lee, D. Wang, Z. Ren, J. Fleurial, and P. Gogna, *Adv. Mater. (Weinheim, Ger.)* **19**, 1043 (2007).
- ⁵T. Borca-Tasciuc, W. Liu, J. Liu, T. Zeng, D. W. Song, C. D. Moore, G. Chen, K. L. Wang, M. S. Goorsky, T. Radetic, R. Gronsky, T. Koga, and M. S. Dresselhaus, *Superlattices Microstruct.* **28**, 199 (2000).
- ⁶S. Chakraborty, C. A. Kleint, A. Heinrich, C. M. Schneider, and J. Schumann, *Appl. Phys. Lett.* **83**, 4184 (2003).
- ⁷B. Yang, W. L. Liu, J. L. Liu, K. L. Wang, and G. Chen, *Appl. Phys. Lett.* **81**, 3588 (2002).
- ⁸G. Joshi, H. Lee, Y. Lan, X. Wang, G. Zhu, D. Wang, R. W. Gould, D. C. Cuff, M. Y. Tang, M. S. Dresselhaus, G. Chen, and Z. Ren, *Nano Lett.* **8**, 4670 (2008).
- ⁹S. T. Huxtable, Ph.D. thesis, University of California–Berkeley, 2002.
- ¹⁰G. Chen, S. Q. Zhou, D.-Y. Yao, C. J. Kim, X. Y. Zheng, Z. L. Liu, and K. L. Wang, *Proceedings of the 17th International Thermoelectrics Conference* (IEEE, New York, 1998), p. 202.
- ¹¹Y. Ezzahri, S. Dilhaire, S. Grauby, J. M. Rampnoux, W. Claeys, Y. Zhang, G. Zeng, and A. Shakouri, *Appl. Phys. Lett.* **87**, 103506 (2005).
- ¹²S. M. Lee, D. G. Cahill, and R. Venkatasubramanian, *Appl. Phys. Lett.* **70**, 2957 (1997).
- ¹³E. S. Landry, M. I. Hussein, and A. J. H. McGaughey, *Phys. Rev. B* **77**, 184302 (2008).
- ¹⁴G. Theodorou, in *Properties of Silicon Germanium and SiGe:Carbon*, edited by E. Kasper and K. Lyutovich (INSPEC, The Institution of Electrical Engineers, London, 2000), pp. 59–62.
- ¹⁵D. E. Jesson, in *Properties of Silicon Germanium and SiGe:Carbon* (Ref. 14), pp. 3–7.
- ¹⁶R. Hull, in *Properties of Silicon Germanium and SiGe:Carbon* (Ref. 14), pp. 9–20.
- ¹⁷G. Chen, *Phys. Rev. B* **57**, 14958 (1998).
- ¹⁸G. Chen and M. Neagu, *Appl. Phys. Lett.* **71**, 2761 (1997).
- ¹⁹D. A. Broido and T. L. Reinecke, *Phys. Rev. B* **70**, 081310(R) (2004).
- ²⁰S. F. Ren, W. Cheng, and G. Chen, *J. Appl. Phys.* **100**, 103505 (2006).
- ²¹S. I. Tamura, Y. Tanaka, and H. J. Maris, *Phys. Rev. B* **60**, 2627 (1999).
- ²²B. Yang and G. Chen, *Nanoscale Microscale Thermophys. Eng.* **5**, 107 (2001).
- ²³P. Hyldgaard and G. D. Mahan, *Phys. Rev. B* **56**, 10754 (1997).
- ²⁴A. A. Kiselev, K. W. Kim, and M. A. Stroschio, *Phys. Rev. B* **62**, 6896 (2000).
- ²⁵M. V. Simkin and G. D. Mahan, *Phys. Rev. Lett.* **84**, 927 (2000).
- ²⁶B. Yang and G. Chen, *Phys. Rev. B* **67**, 195311 (2003).
- ²⁷W. E. Bies, R. J. Radtke, and H. Ehrenreich, *J. Appl. Phys.* **88**, 1498 (2000).
- ²⁸A lattice dynamics–based approach was used by Ren *et al.* (Ref. 20) to model interfacial species mixing in Si/Ge superlattices. This approach is questionable, however, because the interfacial species mixing, which should have no order, is periodically reproduced in the cross-plane direction due to the lattice dynamics framework.
- ²⁹A. A. Abramson, C.-L. Tien, and A. Majumdar, *ASME Trans. J. Heat Transfer* **124**, 963 (2002).
- ³⁰K. Imamura, Y. Tanaka, N. Nishiguchi, S. Tamura, and H. J. Maris, *J. Phys.: Condens. Matter* **15**, 8679 (2003).
- ³¹Y. Chen, D. Li, J. R. Lukes, Z. Ni, and M. Chen, *Phys. Rev. B* **72**, 174302 (2005).
- ³²B. C. Daly, H. J. Maris, K. Imamura, and S. Tamura, *Phys. Rev. B* **66**, 024301 (2002).
- ³³B. C. Daly, H. J. Maris, Y. Tanaka, and S. Tamura, *Phys. Rev. B* **67**, 033308 (2003).
- ³⁴A. J. H. McGaughey, M. I. Hussein, E. S. Landry, M. Kaviani, and G. M. Hulbert, *Phys. Rev. B* **74**, 104304 (2006).
- ³⁵S. Volz, J. B. Saulnier, G. Chen, and P. Beauchamp, *Microelectron. J.* **31**, 815 (2000).
- ³⁶F. H. Stillinger and T. A. Weber, *Phys. Rev. B* **31**, 5262 (1985).
- ³⁷K. Ding and H. C. Andersen, *Phys. Rev. B* **34**, 6987 (1986).
- ³⁸M. Laradji, D. P. Landau, and B. Dunweg, *Phys. Rev. B* **51**, 4894 (1995).
- ³⁹H. Zhao and J. B. Freund, *J. Appl. Phys.* **97**, 024903 (2005).
- ⁴⁰P. K. Schelling, S. R. Phillpot, and P. Keblinski, *Phys. Rev. B* **65**, 144306 (2002).
- ⁴¹P. K. Schelling and S. R. Phillpot, *J. Appl. Phys.* **93**, 5377 (2003).
- ⁴²A. Bodapati, P. K. Schelling, S. R. Phillpot, and P. Keblinski, *Phys. Rev. B* **74**, 245207 (2006).
- ⁴³B. Becker, P. K. Schelling, and S. R. Phillpot, *J. Appl. Phys.* **99**, 123715 (2006).
- ⁴⁴L. J. Porter, J. F. Justo, and S. Yip, *J. Appl. Phys.* **82**, 5378 (1997).
- ⁴⁵The Debye temperatures were obtained by fitting the specific heat (based on a lattice dynamics calculation of the zero-

- temperature phonon density of states) to the Debye model using a least-squares regression analysis.
- ⁴⁶*CRC Handbook of Chemistry and Physics*, 87th ed., edited by D. R. Lide (Taylor & Francis, Boca Raton, FL, 2007), <http://www.hbcpnetbase.com>
- ⁴⁷D. Frenkel and B. Smit, *Understanding Molecular Simulation: From Algorithms to Applications* (Academic, San Diego, 2002).
- ⁴⁸H. J. C. Berendsen, J. P. M. Postma, W. F. van Gunsteren, A. DiNola, and J. R. Haak, *J. Chem. Phys.* **81**, 3684 (1984).
- ⁴⁹We estimate that the simulation cell cross-sectional area would need to be increased by a factor of ~ 40 to model misfit dislocations.
- ⁵⁰D. B. Aubertine and P. C. McIntyre, *J. Appl. Phys.* **97**, 013531 (2005).
- ⁵¹A. J. H. McGaughey and M. Kaviani, in *Advances in Heat Transfer*, edited by G. A. Greene, Y. I. Cho, J. P. Hartnett, and A. Bar-Cohen (Elsevier, New York, 2006), Vol. 39, pp. 169–255.
- ⁵²E. S. Landry, Ph.D. thesis, Carnegie Mellon University, 2009.
- ⁵³In our previous work on Lennard-Jones superlattices, we found the thermal conductivity to be less sensitive to the sample and reservoir lengths than the Si-Ge samples considered here (Ref. [13](#)). This difference is due to the lower thermal conductivity (by 1–2 orders of magnitude) and smaller phonon mean free path of the Lennard-Jones superlattices.
- ⁵⁴T. Ikeshoji and B. Hafskjold, *Mol. Phys.* **81**, 251 (1994).
- ⁵⁵A. Skye and P. K. Schelling, *J. Appl. Phys.* **103**, 113524 (2008).
- ⁵⁶W. Kim, J. Zide, A. Gossard, D. Klenov, S. Stemmer, A. Shakouri, and A. Majumdar, *Phys. Rev. Lett.* **96**, 045901 (2006).
- ⁵⁷W. Kim, R. Wang, and A. Majumdar, *Nanotoday* **2**, 40 (2007).
- ⁵⁸C. Kimmer, S. Aubry, A. Skye, and P. K. Schelling, *Phys. Rev. B* **75**, 144105 (2007).
- ⁵⁹A. J. H. McGaughey and M. Kaviani, *Phys. Rev. B* **69**, 094303 (2004).
- ⁶⁰A. S. Henry and G. Chen, *J. Comput. Theor. Nanosci.* **5**, 1 (2008).
- ⁶¹P. K. Schelling, S. R. Phillpot, and P. Keblinski, *Appl. Phys. Lett.* **80**, 2484 (2002).